Eur. Phys. J. Special Topics **223**, 2131–2144 (2014)
© EDP Sciences, Springer-Verlag 2014
DOI: 10.1140/epjst/e2014-02254-3

THE EUROPEAN PHYSICAL JOURNAL SPECIAL TOPICS

Review

Distribution of chaos and periodic spikes in a three-cell population model of cancer

Auto-organization of oscillatory phases in parameter planes

Michelle R. Gallas[1], Marcia R. Gallas[2,3,4,5,6], and Jason A.C. Gallas[2,3,4,5,6]

[1] Center for Research & Grants, Baptist Health South Florida, Miami, FL 33143, USA
[2] Departamento de Física, Universidade Federal da Paraíba, 58051-970 João Pessoa, Brazil
[3] Instituto de Altos Estudos da Paraíba, Rua Infante Dom Henrique 100–1801, 58039-150 João Pessoa, Brazil
[4] Institute for Multiscale Simulations, Friedrich-Alexander-Universität, 91052 Erlangen, Germany
[5] Max-Planck-Institute for the Physics of Complex Systems, Nöthnitzer Str. 38, 01187 Dresden, Germany
[6] Department of Mathematics, Imperial College London, Huxley Building, 180 Queen's Gate, London SW7 2AZ, UK

Received 11 April 2014 / Received in final form 18 August 2014
Published online 24 October 2014

Abstract. We study complex oscillations generated by the de Pillis-Radunskaya model of cancer growth, a model including interactions between tumor cells, healthy cells, and activated immune system cells. We report a wide-ranging systematic numerical classification of the oscillatory states and of their relative abundance. The dynamical states of the cell populations are characterized here by two independent and complementary types of stability diagrams: Lyapunov and isospike diagrams. The model is found to display stability phases organized regularly in old and new ways: Apart from the familiar spirals of stability, it displays exceptionally long zig-zag networks and intermixed cascades of two- and three-doubling flanked stability islands previously detected only in feedback systems with delay. In addition, we also characterize the interplay between continuous spike-adding and spike-doubling mechanisms responsible for the unbounded complexification of periodic wave patterns. This article is dedicated to Prof. Hans Jürgen Herrmann on the occasion of his 60th birthday.

1 Introduction

For many years a topic of vital importance is the understanding of tumor dynamics and sensitivity to the plethora of factors that determine their manifestation and growth [1,2]. One specific result of the long effort to tame all kinds of tumors is the current availability of a number of mathematical models of tumor dynamics. In one way or another, such models combine tumor growth models (exponential, logistic,

Gompertz, etc.), the response of the immune cells, and terms describing Lotka–Volterra type predator–prey competition for resources among normal and tumor cells. On a more advanced level, models also include terms contemplating molecular-genetic-biological perspectives aiming to account for or to develop specific forms of therapy, particularly chemotherapy.

The study of tumor models is appealing from many points of view. Nowadays, it is attracting considerable interest from the physics community. Dynamically, tumor models open a host of new challenges related to the specific ways of representing complex competition mechanisms, which also underlie other natural phenomena. The situation here is reminiscent of the known Lorenz-Haken isomorphism [3,4] discovered between the irregular pulsations observed in the single-mode laser with the ones known for the Lorenz equations. Since both models operate in completely different regions of the *same* control parameter space, the discovery of the isomorphism has enriched in a single stroke both fields with valuable insight. Interest among the physics community in tumor models is illustrated in papers published, for example, in a special issue dedicated to computational oncology of the Journal of Mathematical Biology [5], and in an ongoing focus issue on the physics of cancer in the New Journal of Physics [6].

From the multitude of models in existence, here we study tumor dynamics as predicted by an interesting three-variables model introduced by de Pillis and Radunskaya [7]. The model in question is an outgrowth of a two-variables model involving a pair of coupled first-order ordinary differential equations introduced by Kuznetsov et al. [8] for two cell populations, namely for effector immune cells and tumor cells. Even for just two cell populations the model could display rich dynamics and explain important aspects of the stages of cancer progression. A valuable asset is that Kuznetsov et al. [8] performed a detailed estimation of parameters describing processes that cannot be measured *in vivo*. They also did a global bifurcation analysis of the two cell model. De Pillis and Radunskaya were interested in exploring how to keep oscillations of cell populations to a minimum and in finding strategies to move the system into the basin of attraction of healthy, stable equilibrium states. They were interested in obtaining a more complete understanding of the implications of the existence of basins of attraction in the treatment process. Both works [7,8] contain long lists of references and nice overviews of the major mathematical frameworks in use, their interpretations, and valuable discussions about the sort of diseases and treatments that they address.

From a dynamical point of view, the typical analysis of cancer models has been mainly confined to phase-space analysis, namely to analysis focused on the variables of the problem, i.e. on recording what happens to the temporal evolution of the variables while keeping parameters fixed, and to identifying and investigating limit sets. The main emphasis of phase-space analysis is to locate and classify fixed points and to perform for them the traditional linear stability analysis with the help of powerful theorems. However, for models involving three or more variables, no theorems are known to ensure or to exclude the existence of periodic/chaotic motions. Phase-space analysis is normally conducted for a selected choice of parameter values. However, modern computer clusters allow one to perform rather detailed investigations and to probe what happens over extended intervals of control parameters. Technically, this means obtaining stability diagrams or, equivalently, phase diagrams. This is what we do here.

Deterministic chaos in the cancer model of de Pillis and Radunskaya was reported recently by Itik and Banks [9]. They found a chaotic attractor for one specific point in parameter space (defined in their Theorem 4.1), calculated Lyapunov exponents for this point, and argued that the system has what they refer to as a Shilnikov-like connection. Their work was complemented and extended by Duarte et al. [10],

who reported finding chaos along one specific parameter interval in control space. These authors characterized chaos using symbolic dynamics and Lyapunov exponents. Concomitantly, Letellier et al. [11] performed a topological analysis of the model, which they find to indicate new trends in understanding interactions among tumor cells. Instead of a single interval, they report chaos for certain parameter intervals of the host cell growth rate and the tumor cell killing rate. In particular, they show that increasing the growth rate of the host cells enhances fluctuations of populations and induces more rare but fast growing tumors. Very recently, Lopez et al. [12] also found chaotic motion for certain parameter choices of the system. By decreasing the response of the immune system to the tumor cells they found a boundary crisis leading to transient chaotic dynamics, so that the system behaves chaotically for a finite amount of time until an unavoidable extinction of the healthy and immune cell populations occurs. They suggested a control method to avoid extinction. Since deterministic chaos is well-documented in Lotka–Volterra type models [13,14], it is curious that it took so long for chaos to be identified in the de Pillis and Radunskaya cancer model.

The aim of the present paper is to considerably extend and complement these previous works by presenting a systematic characterization of the dynamics, chaotic or not, which is observed in two sections of the multiparametric parameter space of the model. Specifically, we report high-resolution phase diagrams displaying a very detailed classification of periodic and chaotic stable oscillations observed in extended two-parameter windows. Such diagrams delimit precisely the (very complex) boundaries between stability phases. Apart from presenting the standard characterization in terms of Lyapunov exponents, we also characterize cell dynamics through the much more illuminating *isospike diagrams*, i.e. phase diagrams depicting for every point in parameter space the number of spikes contained in one period of the regular oscillations [15–20]. As illustrated in the phase diagrams below, in addition to discriminating between chaos and regularity, namely apart from displaying the same informations provided by the usual Lyapunov phase diagrams, isospike diagrams provide two additional key pieces of information. First, their colors display the number of spikes contained in each periodic oscillation, the colorful tiling reflecting the extension and the shape of the phases characterized by stable oscillations having a constant number of spikes. Second, the boundaries between the distinct phases allow one to visualize how the number of spikes of the periodic oscillations evolve when parameters are tuned. In other words, isospike diagrams display the systematic buildup of the number of spikes, i.e. of the complexity of the wave patterns, and how fast and where in the control parameter space the number of spikes accumulate. Of course, such informations can be obtained only through direct numerical simulations.

The next Section describes the model used and details regarding its numerical solution on a large computer cluster. Then, we present and discuss stability diagrams computed for the three cell populations, uncovering several remarkable new dynamical regularities, in particular wide-ranging regularities formed by certain non-spiral networks of shrimps. Another key finding is the discovery of the startling spike unfolding organization summarized in Figs. 6 and 7. Finally, we summarize and digress about a few enticing open problems.

2 The three-cell cancer model and numerical details

The de Pillis-Radunskaya cancer model involves three cell populations, namely the number of N normal, or host, cells, the number T of tumor cells, and the number

I of immune cells. The dynamics of these populations is governed by three coupled ordinary differential equations [7]:

$$\dot{N} = rN(1 - qN) - pTN, \tag{1}$$

$$\dot{T} = aT(1 - bT) - cIT - eTN, \tag{2}$$

$$\dot{I} = s + \frac{\rho IT}{\alpha + T} - \xi IT - \eta I. \tag{3}$$

These equations coincide with Eq. (3) of de Pillis and Radunskaya but have parameters without subindices. The population of normal cells is controlled by the triplet (p, q, r), tumor cells are governed by (a, b, c, e), while immune cells are controlled by $(s, \rho, \alpha, \xi, \eta)$. In the first two equations, r and a control the logistic growth [21,22] of N and T, respectively, while q and b control their corresponding carrying capacities. The constant influx of immune cells is regulated by s, while η defines the death rate in the absence of tumor. The accumulation rate of cytotoxic effector cells is controlled by ρ and α. The remaining parameters define the magnitude of the several nonlinear terms involved. To be meaningful, all parameters need to be non-negative constants. As in previous works, we fix the following reference values: $(p, q, r) = (1.5, 1, 0.6)$, $(a, b, c, e) = (1, 1, 2.5, 1)$, and $(s, \rho, \alpha, \xi, \eta) = (0, 1, 4.5, 0.2, 0.5)$. In the present paper we focus on the dynamics observed in the planes $p \times \xi$ and $r \times \rho$ as highlighted in the equations. As shown below in Fig. 4, the plane $r \times \rho$ displays a surprising number of new dynamical facts.

In the literature, Eqs. (1)–(3) have been ordered in different ways, with parameters named differently, to reflect the particular adimensional form selected for them [9–12]. Here, however, to avoid working with variables that may become singular, we stick to the original unnormalized equations [7]. Obviously, an additional advantage of such equations is that for suitable choice of parameters they may be reduced to all other ones.

The individual phase diagrams given below in Figs. 1–6 record the analysis of oscillations for selected regions of parameter space containing particularly rich dynamics. To produce the diagrams, each parameter window was covered with a mesh of $1200 \times 1200 = 1.44 \times 10^6$ equidistant points. Then, for each point, the temporal evolution was obtained by integrating numerically Eqs. (1)–(3) using the standard fourth-order Runge-Kutta algorithm with fixed time-step $h = 0.01$. In all diagrams, integrations were always performed horizontally from left to right starting from an arbitrarily chosen initial condition, $(N, T, I) = (0.6, 3 \times 10^{-4}, 0.02)$, and proceeding by "following the attractor", namely by using the values of N, T, I obtained at the rightmost end (when finishing the calculation of a horizontal line) to start the calculation for a new horizontal line, after incrementing the parameter vertically [23]. This is a standard way of generating bifurcation diagrams, and the rationale behind it is that, generically, basins of attraction do not change significantly for small changes of parameters thus ensuring a smooth unfolding of the bifurcation curve. Of course, there are also several regions characterized by multistability and no special effort was done to select one specific attractor to mark them. We simply plotted the attractors as found by our algorithm. This procedure has the advantage of allowing one to locate more easily where several stable solutions coexist. In this way, stability diagrams reflect somewhat the intricacies of the underlying basins of attraction.

As usually done, the first 2×10^5 integration steps were disregarded as a transient time needed to approach the attractor, with the subsequent 40×10^5 steps used to compute the Lyapunov spectrum. To find the number of peaks within a period, after computation the Lyapunov exponents we continued integrations for an additional

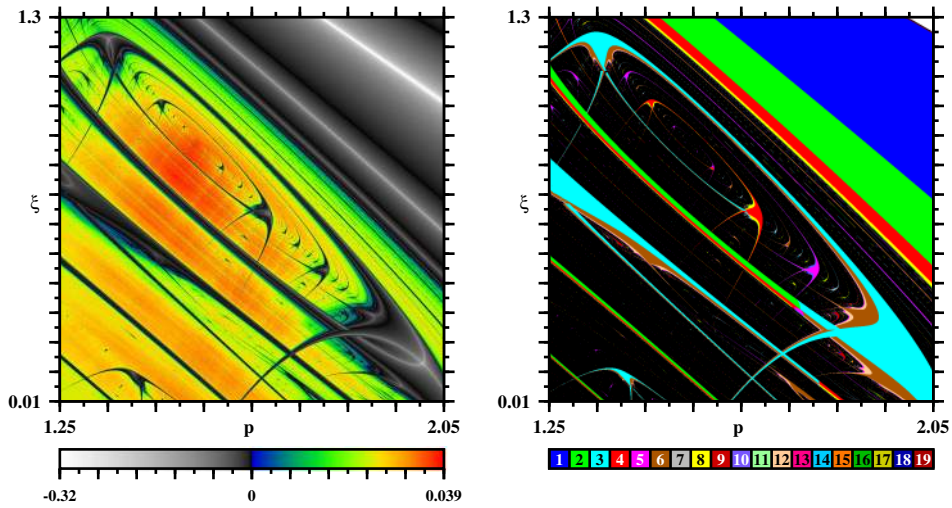

Fig. 1. Two alternative and complementary ways of representing the distribution of stability phases of the cancer model of de Pillis and Radunskaya,illustrating infinite sequences of continuous spiral phases due to stable periodic oscillations. (a) Characterization using Lyapunov exponents: the gray shadings indicate periodic oscillations (i.e. negative exponents), while colors denote chaos (positive exponents). (b) Isospike characterization, colors displaying the number of spikes in one period of N, the population of normal cells. Black regions represent non-periodic oscillations (i.e. chaos). See text. Each panel displays the analysis of $1200 \times 1200 = 1.44 \times 10^6$ individual parameter points.

40×10^5 time-steps recording up to 800 extrema (maxima and minima) of the variable of interest and checking whether pulses repeated or not. The computation of both types of stability diagrams is a standard calculation that we performed as described in detail, e.g., in Ref. [24] where efficient methods to deal with experimental data are also given.

Before proceeding, we mention that the phase diagrams reported here involve extensive computations made possible thanks to specially in-house *ad hoc* developed message-passing programs, and to the decisive help of a SGI Altix cluster with 1536 high-performance processors having a theoretical peak performance of 16 Tflops.

3 Auto-organization of stable phases due to arbitrary oscillations

Figure 1a shows a standard Lyapunov stability diagram, obtained by plotting for the aforementioned very fine parameter grid the largest non-zero Lyapunov exponent. Lyapunov exponents are familiar indicators allowing one to discriminate unambiguously chaos (positive exponents) from periodic oscillations (negative exponents) [25,26]. A very distinct and complementary representation of the same parameter window is presented in Fig. 1b, in the form of an *isospike diagram* [15–20] namely, a diagram obtained by counting the number of peaks (local maxima) contained in one period of the periodic oscillations of a variable of interest, in this figure the population N of normal cells. All isospike diagrams represent spikes using a palette of 19 colors. Solutions having more than 19 spikes were plotted by recycling the 19 basic colors "modulo 19", namely by assigning them a color-index given by the remainder of the integer division of the number of peaks by 19. Multiples of 19 are given the index 19. Black is used to represent chaos (i.e. lack of numerically detectable periodicity/antiperiodicity), white and gold colors mark constant (i.e. non-oscillatory)

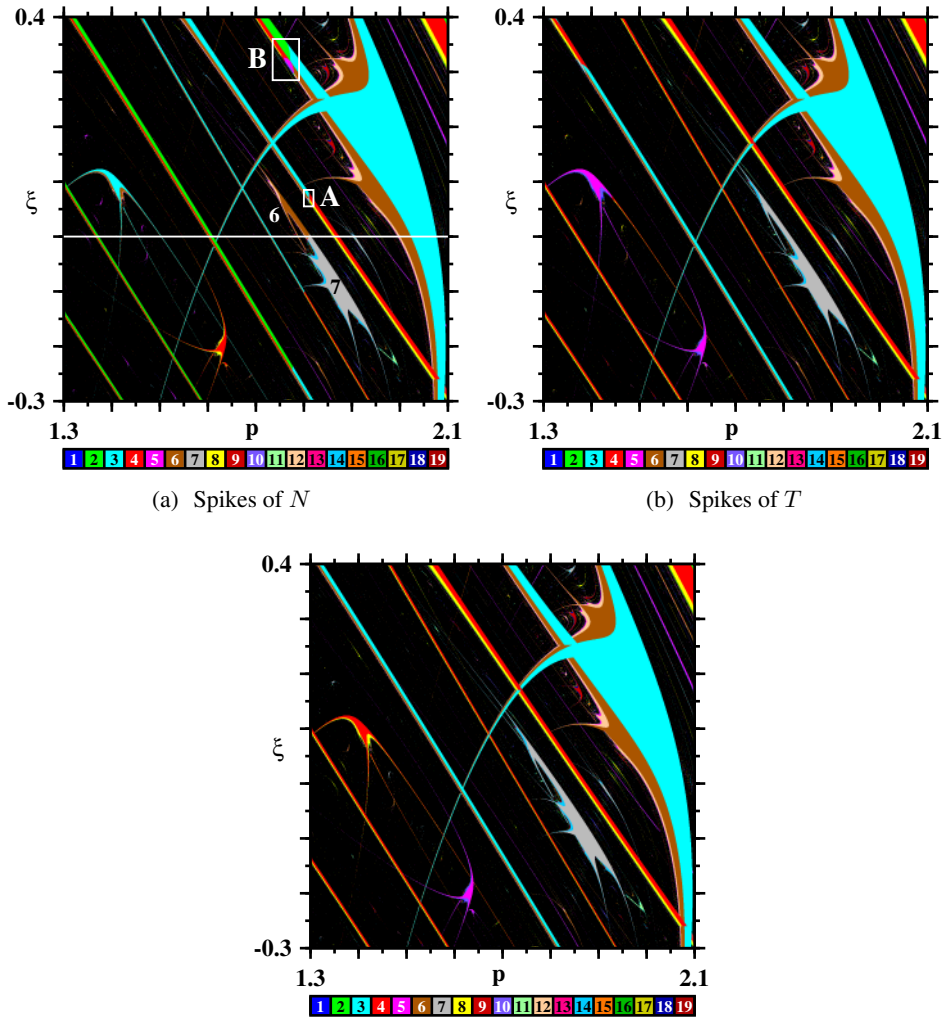

(a) Spikes of N (b) Spikes of T

(c) Spikes of I

Fig. 2. The number of spikes contained in one period of oscillation of the populations of (a) normal cells N, (b) tumor cells T, and (c) immune cells I. Differences in colors show that the number of spikes evolves rather distinctly when parameters are changed. In (a), boxes A and B mark two of the numerous transition regions where the number of spikes increases regularly as shown in Fig. 6a (magnification of box B), Fig. 6b (magnification of box A), and summarized generically in Fig. 6c. Negative parameter values (below the white line) have no meaning for cancer modeling.

solutions, if any, having respectively non-zero or zero amplitudes of the variable under consideration.

Figure 1 shows a first important result: stable oscillations of the cancer model also emerge organized forming infinite sequences of continuous spiral phases of stable periodic oscillations of growing complexity as recently discovered in electronic circuits, in several lasers, in chemical reactions, and in other dynamical systems [27]–[43]. Since the rich dynamics of continuous and discontinuous spiral phases has been described numerically and experimentally in details in a recent survey [24], we do not elaborate

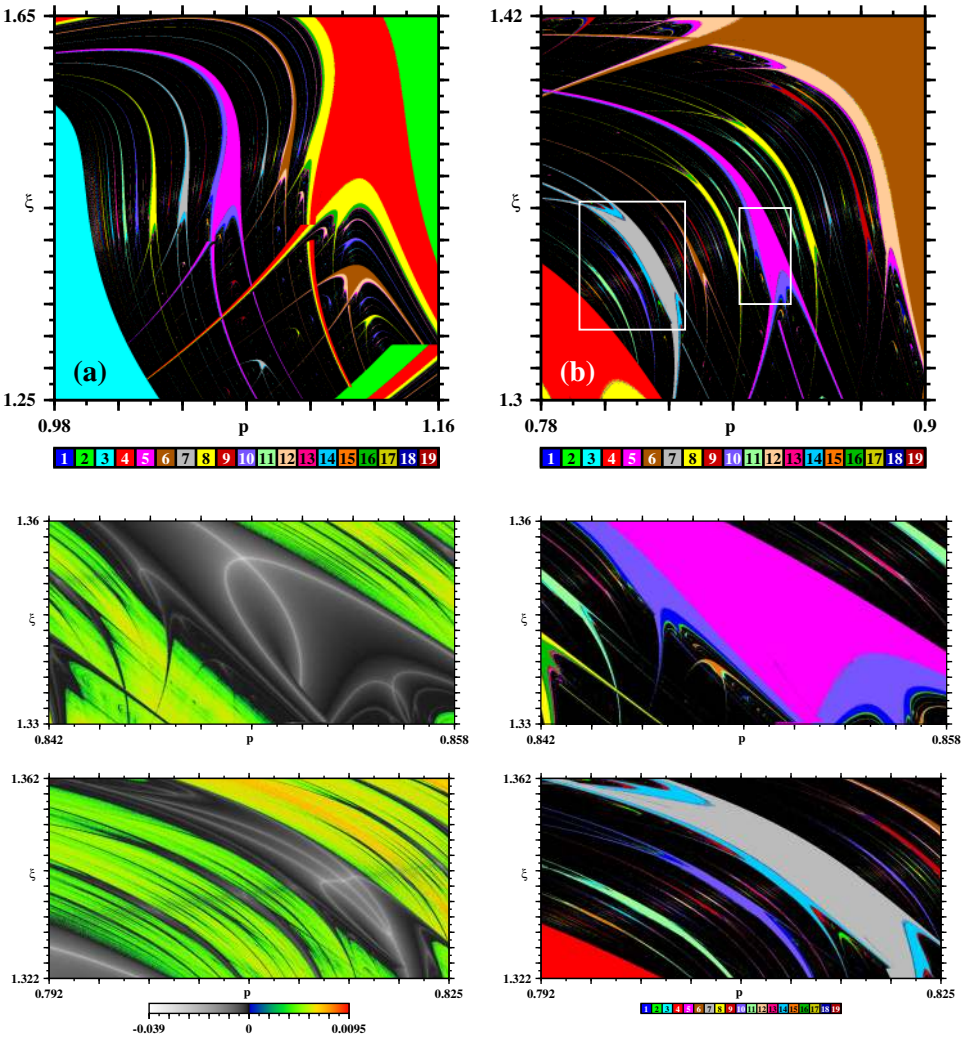

Fig. 3. Stability islands emerge organized forming two distinct sequences. (a) Standard accumulation of *shrimps* [45–49]. (b) Accumulation involving an alternation of two-doubling-flanked shrimps and three-doubling-flanked periodicity islands first observed in Mackey-Glass delay-differential equations [36]. (middle row) (bottom row) Magnifications showing Lyapunov (left) and isospike (right) diagrams for the region contained in the right box in panel (b), illustrating the typical structure of two-doubling-flanked shrimps. (bottom row) Magnifications showing Lyapunov (left) and isospike (right) diagrams for the left box in panel (b), illustrating the typical structure of three-doubling-flanked periodicity islands of systems with delayed feedback [36–38]. The Lyapunov diagrams seen on the left column compare the very distinct inner organization of both structures. See text.

on them here, moving on to focus on new findings. After finishing this work, we found a paper just published by Stegemann and Rech [44] reporting spirals for a Lyapunov diagram equivalent to our $p \times \xi$ diagram seen on the left-hand-side of Fig. 1. We remark that such spirals can be also found in other control planes, e.g. in the $r \times \rho$ plane as seen in Fig. 4 below. As already mentioned, the focus of this paper is on novel networks other than spirals.

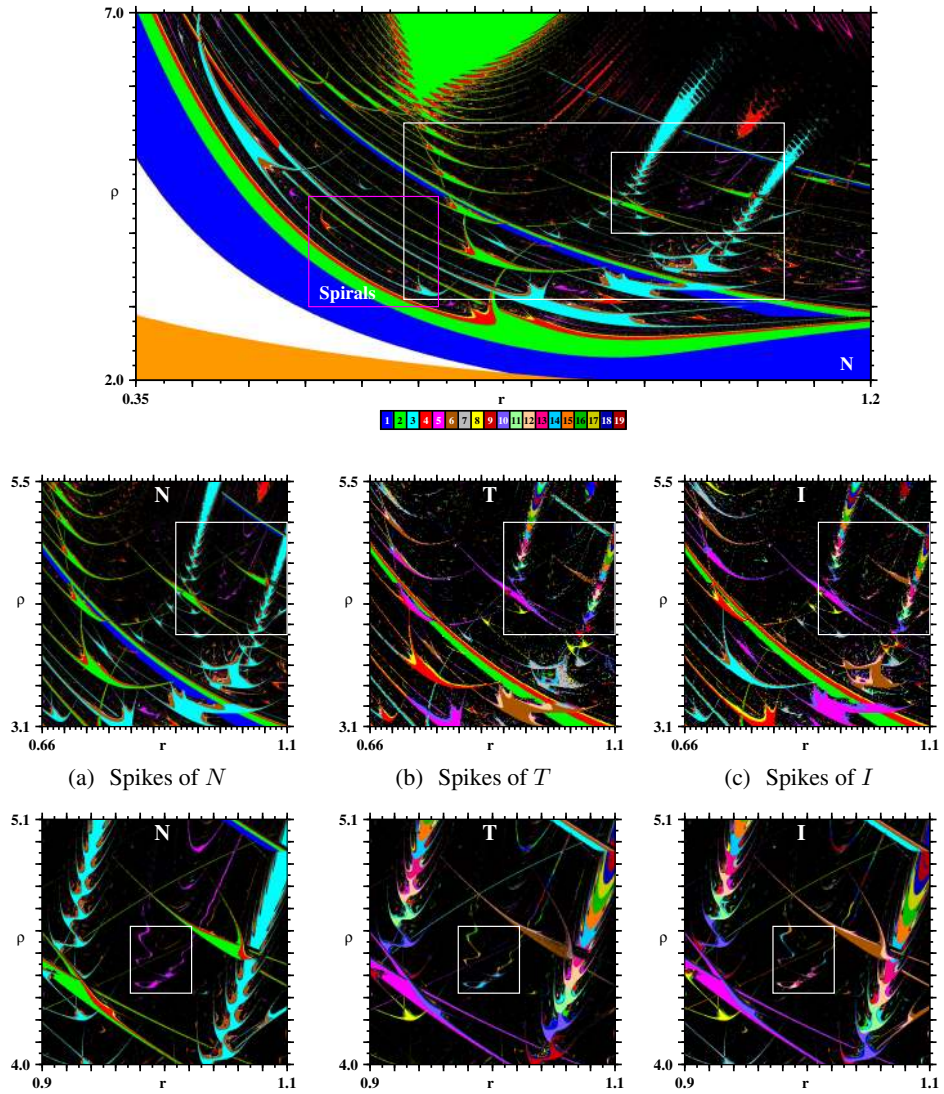

Fig. 4. Phase diagrams illustrating details of zig-zag networks accumulating along very specific directions in control space. The top panel shows a wide region of the control space, characterized here with the spikes detected in the population N of normal cells. The large box seen on the top panel is shown magnified in the middle row, while its inner box seen on the left is shown magnified in the bottom row. The middle row illustrates that number of peaks change regularly but quite differently for N, T, I. Note the presence of continuous spirals inside the leftmost box in the top panel. The boxes in the panels at the bottom row mark birth regions of long ziz-zag networks. This birth is shown magnified in Fig. 5.

Comparing Figs. 1a and 1b one clearly sees that, despite the fact of being derived in rather independent ways, the characterization using the isospike diagram agrees very well with the standard Lyapunov stability diagram. In other words, the Lyapunov diagram can be seen to validate the reliability of the isospike classification, a validation that remains valid for all such diagrams below. Furthermore, comparing Figs. 1a and 1b one sees that isospike diagrams are particularly helpful because, apart from clearly separating periodicity from chaos, they simultaneously display how the

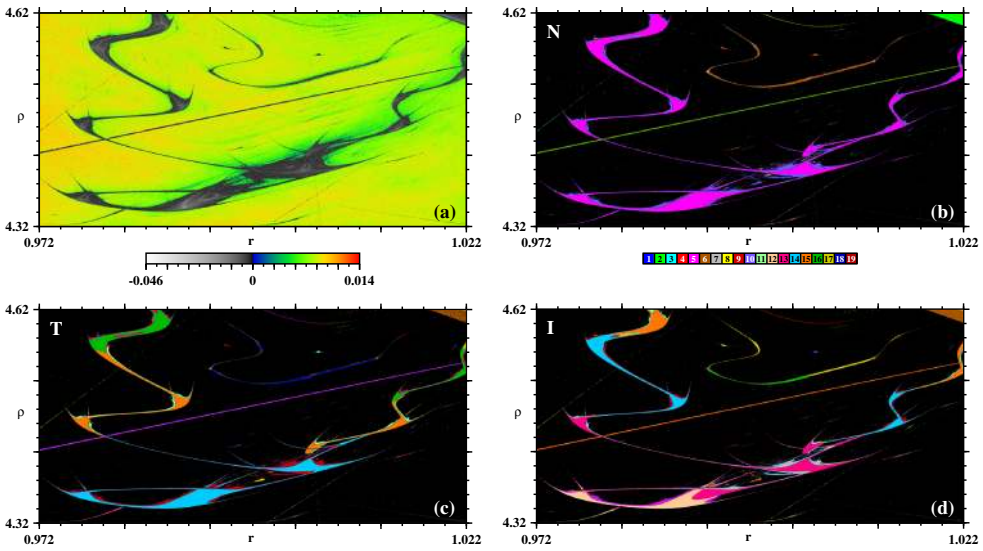

Fig. 5. Details of the genesis of a long zig-zag network, characterized by (a) Lyapunov exponents, and by the number of spikes of periodic oscillations of (b) N, (c) T, and (d) I. While for the population N of normal cells the number of spikes remains constant, a variegated change is seen for the population of tumor and immune cells, which seem to undergo spike changes in a somewhat *drifting synchrony*.

spikes in waveforms of every periodic oscillation evolve as parameters are changed. In other words, they display how the wave patterns of the model get more and more complex when tuning parameter and, simultaneously, how to select parameters to either increase or decrease wave pattern complexity, as desired. Accordingly, in what follows we will mainly use isospike diagrams. We stress, however, that our programs compute both diagrams simultaneously, and we have checked that both diagrams invariably agree.

To count the number of spikes one obviously needs to select a specific variable of the model. A natural question is then to ask whether or not all variables will produce the same counting and, if not, where exactly do the countings differ. For an extended region of parameters, Figure 2 answers both questions. Panel (a) displays the spike distribution for the population of normal cells, (b) for the tumor cells, and (c) for the immune cells. The panels also show negative values of ξ despite the fact that such values have no meaning for the modeling. These negative values are shown here simply to illustrate that the structural distribution of chaos and periodicity changes continuously across the boundary between negative and positive values of ξ, independently of its interpretation in the model. Note that when crossing the boundary between negative and positive parameters in Fig. 2a there is an interchange between 6 and 7 in the number of spikes in N while no interchange is observed for T and I. Analogous interchanges do occur, however, for other values of the parameters. An interesting question discussed below in connection with Fig. 6 is how the number of spikes changes inside the stability phases.

A generic feature that may be easily recognized in Figs. 1 and 2 is the presence of a characteristic alignment along certain directions of the stability islands formed by oscillations having a number of spikes that grow without any bounds. Two such alignments can be seen along a slightly inclined direction in Fig. 3a and along the diagonal in Fig. 3b. In Fig. 3a the alignment involves stability islands having always the same

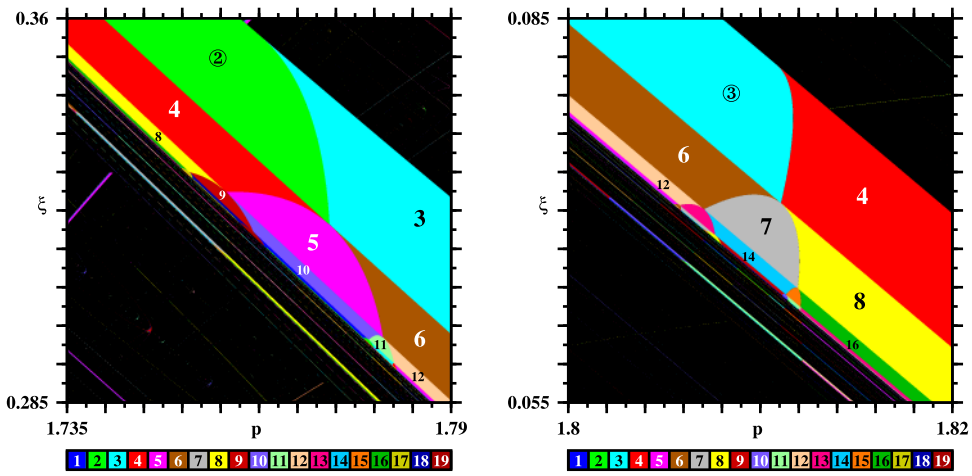

(a) Spikes tree for $p = 2$ (b) Spikes tree for $p = 3$

Fig. 6. Magnifications of the boxes in Fig. 2a displaying representative arborescent patterns created by the smooth interfaces between regions of stable periodic oscillations of N with distinct number of spikes (indicated by the numbers). Peak-adding occurs longitudinally while peak-doubling unfolds transversally. (a) Unfolding beginning with $p = 2$. (b) Unfolding beginning with $p = 3$. Identical unfoldings can be measured in the spikes of T and I, in distinct parameter windows (see Fig. 2).

shrimp shape and structure as well-known for the Hénon map [49]. But the organization shown in Fig. 3a is rather distinct. While shrimps are stability regions flanked by two peak-doubling cascades to chaos, the organization in Fig. 3b consists of an (apparently infinite) alternation of stability phases of two types: the usual shrimps alternate with stability islands flanked by three peak-doubling cascades leading to chaos. This alternation of two- and three-flanked structures was recently observed in the control space of the Mackey-Glass system, a paradigmatic delay-differential equation, namely a considerably more complex model describing a system with delayed feedback and involving infinite degrees of freedom [36]. While the three-flanked structures could be observed for the delayed feedback system, their internal structure was not determined. Here, the inner organization of the superstable-like (white) loci [46,48] seen in the Lyapunov diagrams show unambiguously that two- and three-flanked structures are indeed of a rather distinct kind and they both exist also in low-dimensional sets of ordinary differential equations.

Figure 4a shows a distinct cut of the multidimensional parameter space of Eqs. (1)–(3). This cut was selected because it displays a number of remarkable dynamical facts not seen before. First, the leftmost box in Fig. 4a contains periodicity hubs and infinite sequences of spirals, as described above. This figure shows several sequences of zig-zag networks that were recently reported for electronic circuits containing a tunnel diode and for a laser [41]. While the previously known networks became quickly too small to be observed without considerable magnifications, the cancer model displays in a single picture very clear sequences of very long zig-zag networks. Similarly to Fig. 2 above for distinct parameters, the middle and the bottom panels illustrate the variation of the number of spikes in one period of the populations of N, T, I. The regions containing networks in the panels in these rows show that, while the number of spikes of normal cells maintains a constant number of spikes over very large parameter windows, the spikes counted for tumor and immune cells

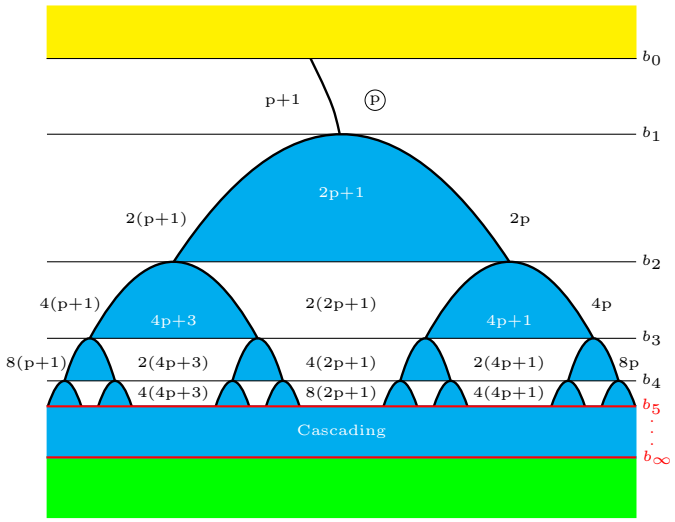

Fig. 7. The generic spikes tree illustrating schematically the regular spike adding and doubling mechanisms. Blue regions always contain odd periods. In the top stripe, the location of the blue region depends of the numerical value of p.

grows systematically. Contemplating the various panels it is possible to recognize the complicated way and the location where the number of spikes change.

Figure 5 shows magnifications of the boxes in the bottom row of Fig. 4. These panels illustrate the peculiar way in which zig-zag networks are born. As before, while the number of spikes in the population of normal cells remains constant over very large ranges, the number of spikes counted in the populations of tumor and immune cells grows without bound. The birth of a larger but more convoluted zig-zag network can be seen in the panel at top of Fig. 4. Additional magnifications (not presented here) show that the inner superstable loci evolve when parameters change, indicating possibly that the zig-zag network may contain other structures than only shrimps, or that the shrimps might be evolving continuously as the network grows. It is also possible that the parameter cut shown in the figure is not optimal to expose the full structure. A detailed analysis of this would, however, involve extended additional computations and is therefore postponed.

Several diagrams above have shown that the number of spikes in N, T, I evolve continuously, changing smoothly and regularly in well-localized regions of the parameter space. Since shrimp-legs contain infinite sequences of spike changes, it is natural to ask how these transitions occur. Two representative examples of such transitions are illustrated in Fig. 6, where the numbers refer to the number of spikes characterizing the region containing them. The figure depicts with more details the sequences of smooth transitions contained in boxes A and B of Fig. 2 and shows that spike-adding occurs longitudinally, i.e. along shrimp legs, while spike-doubling occurs predominantly in the transverse direction.

The unexpected order underlying wave-form complexification by spike adding and doubling is summarized schematically in Fig. 7. In this figure, the two outermost stripes denote regions confining shrimp legs [45–49]. The boundaries b_0 and b_1 on the top define a horizontal stripe $s_0 \equiv b_1 - b_0$ where a *main* spike-number p changes to $p + 1$ along a smooth boundary. In each subsequent stripe $s_k \equiv b_{k+1} - b_k$, for $k = 1, 2, 3, \ldots, \infty$, the number of spikes grows from $2^k p$ to $2^k(p+1)$ by acquiring additional spikes through smooth wave-pattern deformations similar to the ones observed in

infinite dimensional systems involving delayed feedback [36–38]. The spike unfolding illustrated in Fig. 7 is organized in a characteristic tree resembling a bifurcation diagram. This *arborescent* organization may be observed profusely in other regions of the control space, independently of the variable used to count the spikes. This same organization was also observed it in other familiar systems like, e.g. in a tritrophic food chain model, in the Hindmarsh-Rosen model, in a model of neocortical neurons, in a model of a vertical-cavity surface-emitting laser (VCSEL), in a semiconductor laser with injection, in Rössler's oscillator, and in the self-pulsations of a CO_2 laser with feedback (see, for instance, Fig. 1b in Ref. [37]). All these corroborating evidences will be reported elsewhere in due time. Therefore, we believe the spikes tree in Fig. 7 to be a generic and robust property of dissipative flows, a characteristic signature of a systematic wave pattern complexification mechanism acting through spike-adding continuous deformations of periodic oscillations in dissipative nonlinear systems.

4 Conclusions and outlook

We performed a detailed classification of the oscillatory behaviors, periodic or not, supported by a three-cell population cancer model due to de Pillis and Radunskaya. From biparametric stability diagrams interconnecting the populations of normal and immune cells, one may recognize that the model is extremely rich from a dynamical point of view, containing known and many hitherto unknown regularities. By computing phase diagrams for all three model variables, we characterized both the size and shape and the unexpected order underlying the organization of stability phases. Our diagrams show precisely where the number of spikes changes as a function of the cell population used to count them. Interestingly, while spikes in the population of normal cells seems to remain constant over relatively extended parameter windows, the populations of tumor and immune cells display a rich variation and seem to keep a relatively constant difference between their number of spikes. We also found many stability islands which are simply too complicated to be classified systematically or to be described by other means than purely graphically. Incidentally, recall that currently there is no method to locate analytically stability phases for arbitrary oscillations, so that the only way to find them is through direct numerical computations.

The cancer model displays an alternation of two- and three-doubling flanked structures known previously only for infinite-dimensional (delay) dynamical systems. Here, the inner structure of the alternating structures could be clearly differentiated in terms of Lyapunov exponent loci analogous to the well-known superstable loci defined for one-dimensional maps [46]. Novel *comet-like* structures were found abundantly (see Fig. 4). Such wide-ranging parameter connections are potentially interesting to select oscillations with prescribed characteristics of interest. Note that the information in our phase diagrams allows one to effectively *control the dynamics*, namely to select the final dynamical state precisely by performing just a single change of parameters. This is in sharp contrast with conventional methods of controlling the dynamics [50,51], which require pre-investigating unstable orbits, do not include a prescription for the precise selection (targeting) of the final state, and require the permanent application of external perturbations.

There are a number of enticing open problems associated with the stability diagrams reported here. From the point of view of applications, they provide reference charts against which one may compare analogous charts computed for other models and address optimal control therapies. For instance, in the framework of the present model it would be interesting to investigate the effect of a constant influx of immune cells into the system, a process regulated by s in Eq. (3). When neglecting the constant influx of effector cells, Itik and Banks assumed the effector cells to be cytotoxic

T-cells which do not respond to tumor cells unless activated by antigen presenting cells. The activation mechanism of the immune system depends on the antigenicity of the tumors and, to start, seems to justify neglecting the influx of activated effector cells.

de Pillis and Radunskaya associated the long-term behavior of the oscillations according to the basin of attraction in which they start, indicating that the addition of drug terms to the system can move solutions into desirable basins, namely basins characterizing healthy dynamics. Our phase diagrams reveal a great number of situations for which it would be interesting to perform detailed phase-space analysis. Of particular interest are the limit sets of the various parameter accumulations contained in our diagrams. The investigation of different cuts of parameter space remains totally open, in particular the question if both logistic terms produce or not dynamically equivalent stability phases.

In summary, although relatively simple, the nonlinearities underlying the cancer model investigated produce rich and unexpected dynamical facts. Future work should tell if the scenarios found for this model are also present in more sophisticated models which include, e.g. drug resistance or more specific immune cell types. Isomorphically, it would be interesting to check if the novelties found for the cancer model can be traced also in Lotka–Volterra type dynamics. In particular, to look for the beautiful spikes tree of Figs. 6 and 7 in other models.

This work was supported by the Deutsche Forschungsgemeinschaft through the Cluster of Excellence *Engineering of Advanced Materials*, by EU Marie-Curie IRSES Brazilian-European partnership in Dynamical Systems (FP7-PEOPLE-2012-IRSES 318999 BREUDS), and by CNPq, Brazil.

References

1. K. Araki, S. Saji, M.R. Gallas, M. Pegram, Y. Sasaki, Breast Cancer **19**, 95 (2012)
2. J. Liao, M.R. Gallas, M. Pegram, J. Slingerland, Breast Cancer (Dove Med Press) **2**, 79 (2010)
3. H. Haken, Phys. Lett. A **53**, 77 (1975)
4. S. Ayadi, O. Haeberlé, Central European J. Phys. **12**, 203 (2014)
5. M. Chaplain, J. Math. Biol. **58**, 481 (2009)
6. R. Bruinsma, J.F. Joanny, J.A. Käs, Editors, Focus issue on the Physics of Cancer, New J. Phys. (2014)
7. L.G. de Pillis, A. Radunskaya, Math. Comp. Modelling **37**, 1221 (2003)
8. V.A. Kuznetsov, I.A. Makalkin, M.A. Taylor, A.S. Perelson, Bull. Math. Bio. **56**, 295 (1994)
9. M. Itik, S.P. Banks, Int. J. Bif. Chaos **20**, 71 (2010)
10. J. Duarte, C. Januario, C. Rodrigues, J. Sardanyes, Int. J. Bif. Chaos **23**, 1350124 (2013)
11. C. Letellier, F. Denis, L.A. Aguirre, J. Theor. Biol. **322**, 7 (2013)
12. A.G. Lopez, J. Sabuco, J.M. Seoane, J. Duarte, C. Januario, M.A.F. Sanjuan, J. Theor. Biol. **249**, 74 (2014)
13. F. Ercole, S. Rinaldi, *Analysis of Evolutionary Processes* (Princeton University Press, Princeton, 2008)
14. Y. Takeuchi, *Global Dynamical Properties of Lotka–Volterra Systems* (World Scientific, Singapore, 1996)
15. J.G. Freire, J.A.C. Gallas, Phys. Chem. Chem. Phys. **13**, 12191 (2011)
16. J.G. Freire, J.A.C. Gallas, Phys. Lett. A **375**, 1097 (2011)
17. M.A. Nascimento, J.A.C. Gallas, H. Varela, Phys. Chem. Chem. Phys. **13**, 441 (2011)
18. J.G. Freire, T. Pöschel, J.A.C. Gallas, Europhys. Lett. **100**, 48002 (2012)

19. S.L.T. Souza, A.A. Lima, I.R. Caldas, R.O. Medrano-T, Z.O. Guimaães-Filho, Phys. Lett. A **376**, 1290 (2012)
20. A. Hoff, D.T. da Silva, C. Manchein, H.A. Albuquerque, Phys. Lett. A **378**, 171 (2014)
21. C. Obcemea, *Chaotic Dynamics of Tumor Growth, Regeneration*, Chapter 34, in *Unifying Themes in Complex Systems*, edited by A.A. Minai, Y. Bar-Yam (Springer, New York, 2006)
22. Z. Bajzer, S. Vuk-Pavlovic, M. Huzak, *Mathematical Modeling of Tumor Growth Kinetics*, Chapter 3, in *A Survey of Models for Tumor-Immune System Dynamics*, edited by J.A. Adams, N. Bellomo (Birkhäuser, Boston, 1997)
23. J.G. Freire, R.J. Field, J.A.C. Gallas, J. Chem. Phys. **131**, 044105 (2009)
24. A. Sack, J.G. Freire, E. Lindberg, T. Pöschel, J.A.C. Gallas, Nature Sci. Rep. **3**, 3350 (2013)
25. R. Kautz, *Chaos: The Science of Predictable Random Motion* (Oxford University Press, Oxford, 2011)
26. T. Tél, M. Gruiz, *Chaotic Dynamics: An Introduction Based on Classical Mechanics* (Cambridge University Press, Cambridge, 2006)
27. C. Bonatto, J.A.C. Gallas, Phys. Rev. Lett. **101**, 054101 (2008)
28. J.G. Freire, J.A.C. Gallas, Phys. Rev. E **82**, 037202 (2010)
29. J.A.C. Gallas, Int. J. Bifurc. Chaos **20**, 197 (2010)
30. R. Vitolo, P. Glendinning, J.A.C. Gallas, Phys. Rev. E **84**, 016216 (2011)
31. R. Barrio, F. Blesa, S. Serrano, A. Shilnikov, Phys. Rev. E **84**, 035201 (2011)
32. R. Barrio, A. Shilnikov, L.P. Shilnikov, Int. J. Bif. Chaos **22**, 1230016 (2011)
33. R. Stoop, P. Banner, Y. Uwate, Phys. Rev. Lett. **105**, 074102 (2010)
34. C. Bonatto, J.C. Garreau, J.A.C. Gallas, Phys. Rev. Lett. **95**, 143905 (2005)
35. C. Bonatto, J.A.C. Gallas, Y. Ueda, Phys. Rev. E **77**, 026217 (2008)
36. L. Junges, J.A.C. Gallas, Phys. Lett. A **376**, 2109 (2012)
37. L. Junges, J.A.C. Gallas, Opt. Comm. **285**, 4500 (2012)
38. L. Junges, T. Pöschel, J.A.C. Gallas, Eur. Phys. J. D **67**, 149 (2013)
39. H.A. Albuquerque, P.C. Rech, Int. J. Circuit Theory Appl. **40**, 189 (2012)
40. C. Cabeza, C.A. Briozzo, R. Garcia, J.G. Freire, A. Marti, J.A.C. Gallas, Chaos Sol. Frac. **52**, 59 (2013)
41. R.E. Francke, T. Pöschel, J.A.C. Gallas, Phys. Rev. E **87**, 042907 (2013)
42. V. Kovanis, A. Gavrielides, J.A.C. Gallas, Eur. Phys. J. D **58**, 181 (2010)
43. J.G. Freire, C. Cabeza, A. Marti, T. Pöschel, J.A.C. Gallas, Nature Sci. Rep. **3**, 1958 (2013)
44. C. Stegemann, P.C. Rech, Int. J. Bif. Chaos **24**, 1450023 (2014)
45. E.N. Lorenz, Physica D **237**, 1689 (2008)
46. W. Façanha, B. Oldeman, L. Glass, Phys. Lett. A **377**, 1264 (2013)
47. J.A.C. Gallas, Appl. Phys. B **60**, S-203 (1995)
48. J.A.C. Gallas, Physica A **202**, 196 (1994)
49. J.A.C. Gallas, Phys. Rev. Lett. **70**, 2714 (1993)
50. *Handbook of Chaos Control*, edited by E. Schöll, H.G. Schuster (Wiley-VCH, Weinheim, 2007)
51. *Introduction to Control of Oscillations and Chaos*, edited by A.L. Fradkov, A.Yu. Pogromsky (World Scientific, Singapore, 1999)